Composite Optical Vortices Formed by Collinear Laguerre-Gauss Beams

E.J. Galvez, N. Smiley, and N. Fernandes

Department of Physics and Astronomy, Colgate University, 13 Oak Drive, Hamilton, New York 13346, U.S.A.

ABSTRACT

We study the optical fields that are produced when two Laguerre Gauss beams, each carrying an optical vortex, are superimposed collinearly. We find that the resulting beam contains new vortices. The number of vortices and their location depends on the charge of the vortices of the component beams and the relative intensity of the two beams. Our presentation focuses on the cases where the component Laguerre-Gauss beams are of order one and two.

Keywords: Singular optics, Optical Vortices, Laguerre-Gauss Beams, Orbital Angular Momentum

1. INTRODUCTION

The study of optical beams bearing phase singularities is interesting from fundamental and applied perspectives. Rich in physical phenomena, optical singularities provide an important setting for discovering new wave phenomena.[1] The angular momentum carried by beams with phase vortices also adds a new dimension to the topic. Phase vortices have their main application in the transfer of orbital angular momentum from light to matter in optical tweezers.[2] More recently, it has been shown that the quantization of this angular momentum has the potential for encoding multiple quantum bits of information.[3]

Recent research on optical vortices has revealed novel results on the propagation of vortex structures, with findings such as the knotting of vortex filaments.[4,5] The optical wave field in these studies was created by the superposition of beams that contain fundamental phase singularities, such as Laguerre-Gauss (LG) beams. Thus, the study of the superposition of beams bearing fundamental vortices is an important step for a better understanding of the problem. A recent numerical study of the superposition of LG beams of the same order showed an interesting redistribution of the phase vortices as a function of the lateral displacement of the two beams.[6] Here we study both theoretically and experimentally the optical fields that result when we combine two LG beams of different order. In contrast to the previous work, we keep the two component LG beams collinear, but vary other parameters, such as the order of the components and their relative intensity. We examine the two cases where one component LG beam is of order one and the other beam is of order two.

This article is organized as follows. In Sec. 2 we present analytical and computational analyses of the problem. Section 3 describes the experimental technique that we used to produce and diagnose the composite wave fields, and in Sec. 4 we present the imaging of the composite beams.

2. THEORY

Let μ_p^ℓ be the field of an LG beam of order $N = 2p + |\ell|$, where p and ℓ are the radial and azimuthal indices, respectively. If we consider the case where $p = 0$, then the field distribution of the beam is a single ring that contains a phase vortex of charge ℓ at its center. The normalized field in this beam is given by[7]

$$\mu_0^\ell = (\frac{2}{\pi|\ell|!})^{1/2}\frac{1}{w}(\frac{r\sqrt{2}}{w})^{|\ell|}e^{-r^2/w^2}e^{-i\ell\phi}e^{i[kz-kr^2/(2R)]}e^{i\varphi}, \tag{1}$$
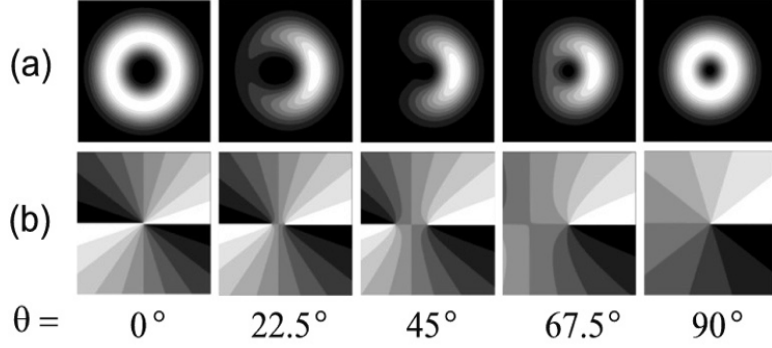
Figure 1. Simulations of a composite optical vortex beam made of component beams with $\ell_1 = +1$ and $\ell_2 = +2$. Row (a) shows the distribution of intensity on a gray scale, going from low (black) to high (white) intensity. Row (b) shows the phase of the field; the gray scale varies from white representing a phase of zero to black representing 2π. The angle theta specifies the relative weight of the two component vortices, as determined by Eq. 2.

where r, ϕ and z are the cylindrical coordinates, w is the beam radius, k is the wave number, R is the radius of curvature of the wave-front, $\varphi = (N+1)\tan^{-1}(z/z_R)$ is the Gouy phase, and z_R is the Raleigh range.

Now consider the collinear superposition of two LG beams with charge ℓ_1 and ℓ_2. Let us set $|\ell_2| > |\ell_1|$. The total field is given by

$$\mu_T = \sin\theta\, \mu_0^{\ell_1} + \cos\theta\, \mu_0^{\ell_2} e^{i\delta}, \tag{2}$$

where δ is the relative phase between the two beams and θ is a parameter that specifies the relative weight of the two beams. The location of the phase vortices in this field is obtained by finding the points (r,ϕ) where μ_T meets the conditions:[8]

$$\mathrm{Re}(\mu_T) = 0 \tag{3}$$
$$\mathrm{Im}(\mu_T) = 0. \tag{4}$$

We find that the solution yields a vortex of charge ℓ_1 located at $r = 0$, and $|\ell_2 - \ell_1|$ vortices of charge $\ell_2/|\ell_2|$ located at positions specified by the coordinates (r,ϕ), where

$$r = \frac{w}{\sqrt{2}}\left(\sqrt{\frac{|\ell_2|!}{|\ell_1|!}}\tan\theta\right)^{1/(|\ell_2|-|\ell_1|)}, \tag{5}$$

and

$$\phi = \frac{\delta + n\pi}{\ell_2 - \ell_1}, \tag{6}$$

with n being an odd integer.

It is interesting to understand how this works. The variable θ defines the weight of each component beam. When $\theta = 0$ it is purely an ℓ_2-vortex beam, and when $\theta = \pi/2$ it is purely an ℓ_1-vortex beam. That is, at these two extremes the beam is composed of a vortex located at the center of the beam, per definition of the Laguerre-Gauss beams in Eq. 1. For values of θ between 0 and $\pi/2$ the beam profile has a much more complex structure. It is consistent with the following view: at $\theta = 0$ we have a central ℓ_2 vortex that is composed of the ℓ_1 vortex superimposed with $|\ell_2 - \ell_1|$ singly charged vortices with a combined charge $\ell_2 - \ell_1$. As θ is increased from zero, the $|\ell_2 - \ell_1|$ vortices move away from the center of the beam reaching their limiting positions at $\theta = \pi/2$, where $r = \infty$. Thus, at this limit there is a single vortex of charge ℓ_1 at the center of the beam.

We have verified the solution presented above with numerical calculations of the total field in a transverse plane of the beam. For simplicity these calculations assumed $z = 0$, which imply $R = \infty$ and $\varphi = 0$. The calculated two-dimensional images, shown in Figs. 1 and 2, also allow a better appreciation of the structure of the composite beams. Each simulation is displayed in a two-dimensional frame of length $4w$.
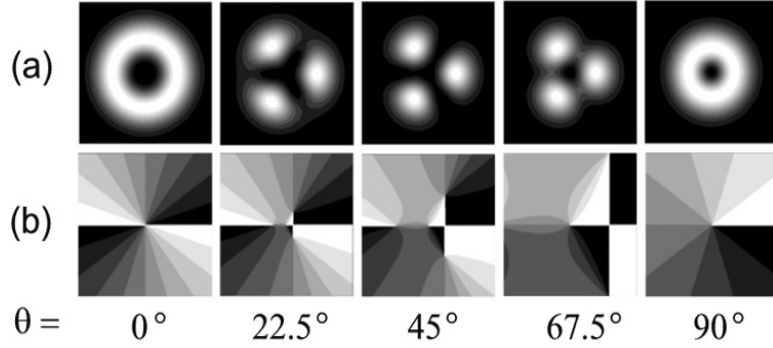
Figure 2. Simulations of a composite optical vortex beam made of component beams with $\ell_1 = +1$ and $\ell_2 = -2$. Row (a) shows the distribution of intensity on a gray scale, going from low (black) to high (white) intensity. Row (b) shows the phase of the field; the gray scale varies from white representing a phase of zero to black representing 2π. The angle theta specifies the relative weight of the two component vortices, as determined by Eq. 2.

Let us start with the simplest situation that we have found: $\ell_1 = +1$ and $\ell_2 = +2$. The calculations can be seen in Fig. 1, which displays in row (a) the intensity profile of the beam, and in row (b) the phase of the field. In both types of images we have deliberately discretized the gray scale to appreciate better the intensity and phase contours. One step in the gray scale corresponds to one tenth of the full scale. Thus, in the case of the phase plots each step of the gray scale corresponds to a phase increment of $\pi/5$. The convention for the sign of the vortex is the following: a vortex charge is positive when the shading increases in darkness when going in a counter clockwise manner around the vortex (e.g., the phase plots for $\theta = 90°$ in Figs. 1 and 2 contain a single $+1$ vortex).

The analytical solution for this case specifies that there are two $+1$ vortices. At $\theta = 0$ they are both at $r = 0$. As θ increases from zero we see one $+1$ vortex moving linearly away from the center of the beam. It is interesting to see that as θ increases the intensity pattern opens up giving the appearance of expelling the $+1$ vortex, and closing back up once the leaving vortex is away from the center. Notice that the intensity pattern is very sensitive to the location of the leaving vortex: at $\theta = 67.5°$ this vortex is at $r = 2.4w$, and thus is outside of the plot frame, and in a location where the intensity of the beam is negligibly small. However, despite this the intensity distribution of the beam remains highly asymmetric. When $\theta = 90°$ the beam is left with a $+1$ vortex at its center.

In the computations of Figs. 1 and 2 we set the relative phase δ between the two beams to zero. The orientation of the pattern depends on δ: as δ is varied the entire pattern rotates about the center of the beam. We used this feature in the laboratory to align the component beams collinear.

The case where $\ell_1 = +1$ and $\ell_2 = -2$ is much more interesting. The solution specifies a $+1$ vortex at $r = 0$ with three -1 vortices moving radially outwards as θ is increased from zero. When $\theta = 22.5°$ and $\delta = 0$, Eqs. 5 and 6 predict three -1 vortices located at the radial distance $r = 0.41w$ and symmetrically oriented at the angles $\phi = \pi/3$, $\phi = \pi$ and $\phi = 5\pi/3$. This analytical solution is verified by the calculations of Fig. 2. The retreating vortices are more obvious when $\theta = 45°$. As shown in row (a) of Fig. 2, the intensity is zero at the locations of the vortices.

Let us analyze the phase variation in Fig. 2. Although the pattern should be symmetric under a rotation of $2\pi/3$, the discretization of the gray scale introduces some minor artificial asymmetries. It is interesting to note that the phase variation around the vortices is not uniform. The phase gradient is highest along the lines that connect the vortices. It is also interesting that in the regions of non-zero intensity the phase is not constant, and the gradient of the phase depends on the value of θ.

We have also investigated other possibilities. Similar behavior is observed for other values of ℓ_1 and ℓ_2. When $|\ell_2 - \ell_1| = 1$ one singly charged vortex moves radially away from the center of the beam for increasing values of θ, leaving a vortex of charge ℓ_1 at the center. This behavior is similar to the first case that we discussed.
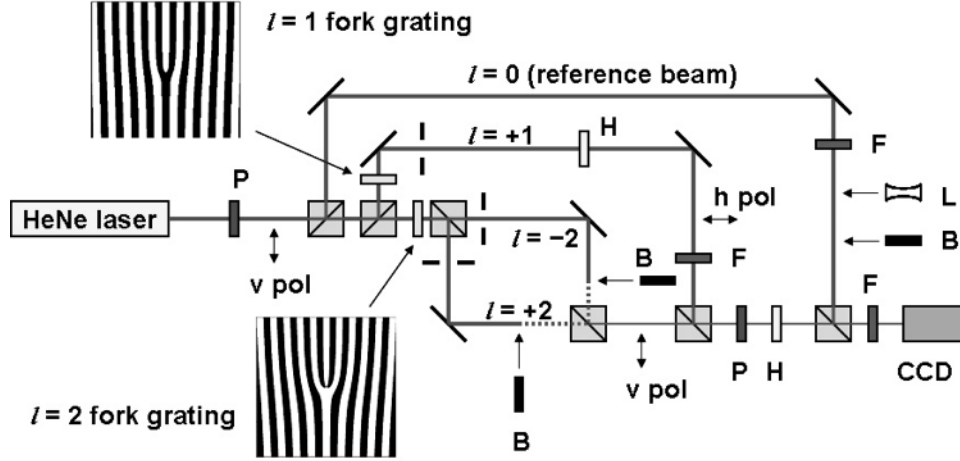
Figure 3. Optical layout of the apparatus to study composite optical vortices. Beams with $\ell_2 = -2$ and $\ell = +1$ vortices are produced by forked diffraction gratings and superposed in a Mach-Zehnder interferometer. Individual components shown explicitly are half-wave plates (H), polarizers (P), beam blockers (B), lens (L) and neutral-density filters (F).

When $|\ell_2 - \ell_1| > 1$ the composite vortices are arranged symmetrically about the center of the beam, and moving radially away from it as θ is increased. This is similar to the second case discussed above.

When the two beams have the same order (i.e., $\ell_1 = -\ell_2$) *no new vortices appear*. In these cases only the center of the beam has a vortex, if any. Then as θ is varied only the phase readjusts. For $\theta < \pi/4$ the phase increases nonlinearly and the intensity distributes into $2|\ell_2|$ lobes. The phase increases in the sense of the dominant singularity ℓ_2, with its gradient being highest in the regions between the lobes. When $\theta = \pi/4$ the regions between the lobes become radial nodes, and the phase jumps discontinuously by π at the node lines. Thus, at this value of θ the central phase singularity disappears and the nodes contain shear phase singularities. For $\theta > \pi/4$ the continuous phase gradients reappear but in the opposite sense, signaling the prevalence of the oppositely-charged phase vortex (i.e., ℓ_1). A common example of this is the case where $\ell_2 = +2$ and $\ell_1 = -2$. When $\theta = \pi/4$ they give rise to a mode that has four lobes, which turns out to be the well known Hermite-Gauss mode "11" (i.e., TEM_{11}).[7,9]

3. EXPERIMENTAL ARRANGEMENT

The optical setup used to perform the experiments consisted of several nested interferometers. Figure 3 shows a schematic of the optical layout. A light beam from a HeNe laser was split by 50-50 non-polarizing beam splitter cubes into four beams. After preparation into the desired LG modes, the beams were recombined coherently downstream via a second set of non-polarizing beam splitters. A charge-coupled-device (CCD) camera imaged the final beam.

The incident beam was prepared to be linearly polarized along a vertical plane. The first beam that split off the main laser beam was used as a diagnosis tool in the preparation of the individual LG beams. In a second role, it was expanded with a diverging lens and deliberately misaligned. The resulting beam was used to create a fringe interference pattern with the composite beam. This served to identify the optical vortices, as described below.

The second beam that split off the main beam from the laser was sent to a computer-generated charge-1 forked binary amplitude grating. A steering mirror and an iris placed after the grating were used to select the $\ell = +1$ beam. A half-wave plate (H in Fig. 3) placed in the path of the beam rotated its polarization by 90 degrees.

The light that remained in the main beam axis continued to a charge-2 forked diffraction grating. A Mach-Zehnder interferometer placed after it was used to channel the first-order, $\ell = +2$ and $\ell = -2$, LG beams to each
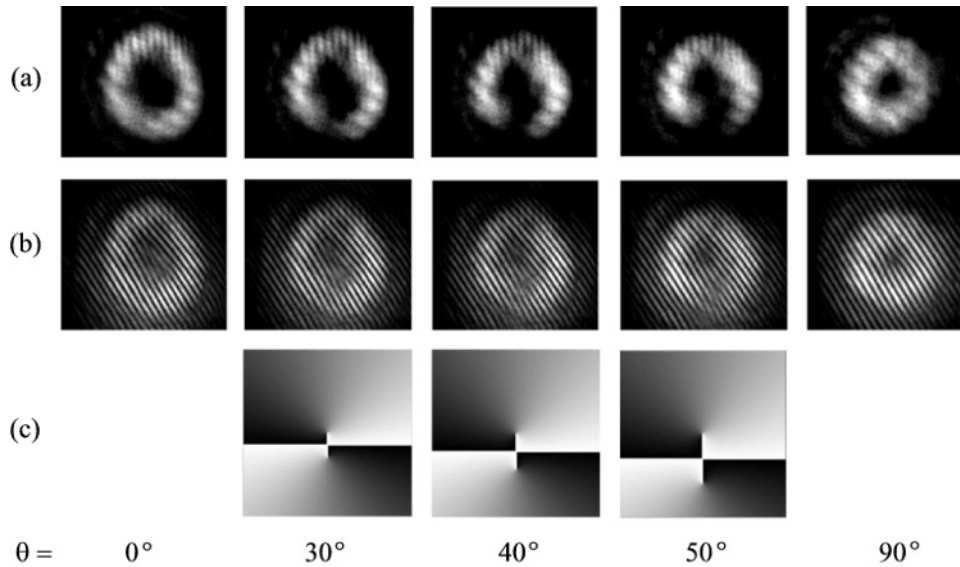
Figure 4. Images of the composite beams for the case where $\ell_1 = +1$ and $\ell_2 = +2$. Row (a) shows images of the composite beam, row (b) shows the interference of the composite beam with a tilted and expanded reference beam, and row (c) shows the phase computations with the phase between the component beams δ adjusted to match the experimental image.

of its arms. For the experiments reported here we selected one of the $|\ell| = 2$ beams by putting a beam block (B in Fig. 3) in the appropriate arm of the interferometer. The pure LG beams were diagnosed by interference with the $\ell = 0$ reference beam; the gratings were mounted on XY translation stages so they could be centered on the beam without affecting the beam alignment.

The vertically polarized $|\ell| = 2$ beam was combined with the horizontally polarized $\ell = +1$ beam with a non-polarizing beam splitter. The intensities of each beam were adjusted to be equal by means of neutral density filters (F in Fig. 3). The two beams with polarizations orthogonal to each other were made interfere by projecting them along the same polarization plane with a linear polarizer. The polarizer (P in Fig. 3) had its transmission axis oriented an angle θ relative to the vertical. It is interesting that because of the axial phase of both beams, the intensity of the resulting beam remained the same regardless of the value of θ. This served as a useful tool for adjusting the relative intensity of the beams while keeping the total intensity constant.

The resulting beam, called hereafter the signal beam, was attenuated by neutral density filters and imaged by the CCD camera. A critical aspect of the alignment was the combination of the two component beams. We used the inherent symmetry of the patterns as an aid in their alignment. One of the mirrors steering the ℓ_1 beam was mounted on a translation stage that had a piezo-electric ceramic as a spacer. As a voltage applied to the piezo-electric was increased, the position of the mirror mounted on the stage was changed slightly, changing the phase δ between the two component beams. This feature allowed the observation of the signal beam as a function of δ. If the beams were aligned perfectly collinear then the resulting pattern rotated about the axis of the beam as δ was changed.

To locate the position of the composite optical vortices we imaged the fringe pattern formed by the interference of the signal beam with the reference beam. For maximum contrast, the polarization of the signal beam was rotated to be in the same (vertical) plane as the polarization of the reference beam. We did this rotation by means of a half-wave plate. Phase vortices appeared as forks in the images, as will be shown in the next section.

4. RESULTS

Figure 4 shows a sequence of images for the case where the vortices of the component LG beams were $\ell_2 = +2$ and $\ell_1 = +1$. Row (a) shows images of the composite beams for different settings of θ. Row (b) shows the
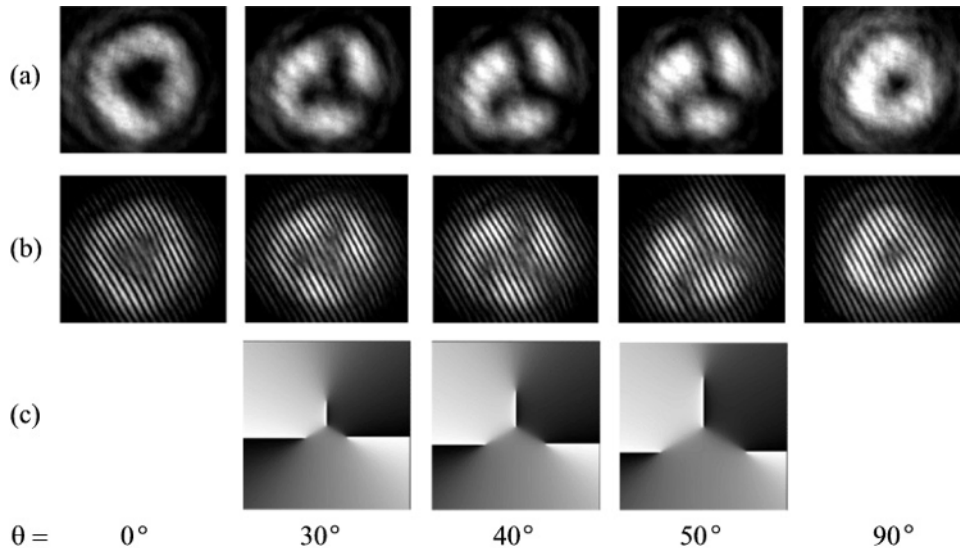
Figure 5. Images of the composite beams for the case where $\ell_1 = +1$ and $\ell_2 = -2$. Row (a) shows images of the composite beam, row (b) shows the interference of the composite beam with a tilted and expanded reference beam and row (c) shows the phase computations with the phase between the component beams δ adjusted to match the experimental image.

interference patterns of the reference beam with the corresponding composite beam. In row (c) we display the phase plots for the corresponding cases; this time with a gray scale of 100 steps. The reader must not get distracted by the sharp white/black boundaries. They represent a step of $\pi/50$. One can identify the vortices by the forks that appear in the interference pattern. The sign of the vortex is specified by the orientation of the forks in the figure: a positive charge appears as a fork with the fork tines pointing toward the lower right.

When $\theta = 0$ we see two $+1$ forks in the central area of the image. We do not observe the expected single $+2$-charge fork. Although we have not investigated this in great detail, we speculate that it might be due to slight deviations of the component beams from the ideal LG form caused by the transmission of the beams through imperfect optical elements.

The images in Fig. 4 show qualitatively the expected changes in the positions of the vortices when θ was increased. A similar confirmation is observed in Fig. 5, for the case where $\ell_1 = +1$ and $\ell_2 = -2$. The values of θ chosen for both figures correspond to images that exhibit appreciable changes in the locations of the vortices. Note the correlation between the orientation of the forks and the expected sign of the vortices. Because of the coarse size of the forks we were not able to make a stringent quantitative comparison of the vortex locations with the theoretical predictions.

Figure 6 shows a blown-up image of the interference pattern for the case where $\ell_1 = +1$ and $\ell_2 = -2$. Three forks of charge -1 appear at the ends of a tilted "Y", with a fork of charge $+1$ located at its center. The lack of perfect symmetry is due to a slight misalignment of the component beams. The figure also allows one to appreciate the limitations of this method of imaging the vortices: the uncertainty in the position of the forks is a significant fraction of their radial position.

5. SUMMARY AND CONCLUSIONS

In summary, we have studied both experimentally and theoretically the composite vortices that arise when two high-order LG beams bearing optical vortices are combined collinearly. For component beams of different order we observe the creation of new vortices, which appear at locations determined by the value of the charge of the component beams and their relative intensity. We find the arrangement of composite vortices to follow a universal pattern. At the center of the beam there is a vortex of charge equal to the one of the component beam
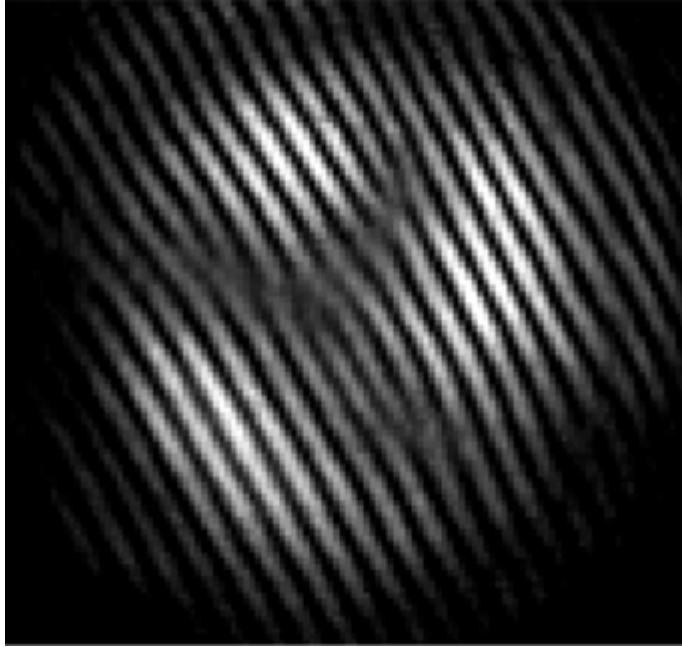
Figure 6. Images of an interference pattern between the composite beam for the case $\ell_1 = +1$ and $\ell_2 = -2$ when $\theta = 45°$, and the $\ell = 0$ reference beam.

that has the lowest charge magnitude, surrounded by one or more singly-charged vortices. The total charge of all the vortices, including the central one, adds to the charge of the component beam that has the greatest charge magnitude.

When the composite beams are of the same order our calculations show that no new vortices appear. Rather, the phase distributes unevenly around the central vortex. When the weights of the two beams are equal the central singularity disappears, giving rise to shear phase singularities.

This work was limited to the case of two collinear component beams. It will be interesting to extend this work to the systematic study of the non-collinear case. In such a case we expect to find the composite vortices in non symmetric arrangements. Other possibilities for further work include the combination of more that two beams, where the created vortices may not be singly charged. Although the number of parameters is larger than the case studied here, the resulting patterns may be richer.

ACKNOWLEDGMENTS

REFERENCES

1. M.V. Berry, "Much Ado About Nothing: Optical Dislocation Lines (Phase Singularities Zeros, Vortices...)," in *Singular Optics*, M.S. Soskin (ed.), *Proc. SPIE* **3487** pp. 1-5, 1998.
2. H. He, M.E. Friese, N.R. Heckenberg, and H. Rubinsztein-Dunlop, "Direct observation of transfer of angular momentum to absorptive particles from a laser beam with a phase singularity," *Phys. Rev. Lett.* **75**, pp. 826–829, 1995.
3. A. Mair, A. Vaziri, G. Welhs, and A. Zeilinger, "Entanglement of the Orbital Angular Momentum States of Photons," *Nature*, **412**, pp. 313–316, 2001.
4. M.V. Berry and M.R. Dennis, "Knotting and Unknotting of Phase Singularities: Helmholtz Waves, Paraxial Waves in 2+1 Spacetime," *J. Phys. A: Math. Gen.* **34**, pp. 8877–8888, 2001.

5. J. Leach, M.R. Dennis, J. Courtial and M.J. Padgett, "Vortex Knots in Light," *New J. Phys.* **7**, pp. 1–11, 2005.

6. I.D. Maleev and G.A. Swartzlander, Jr., "Composite Optical Vortices," *J. Opt. Soc. Am. B* **20**, pp. 1169–1176, 2003.

7. M.W. Beijersbergen, L. Allen, H.E.L.O. van der Veen, and J.P. Woerdman, "Astigmatic Laser Mode Converters and the Transfer of Orbital Angular Momentum," in *Opt. Commun.* **96**, pp. 123–132, 1993.

8. M.V. Berry and M.R. Dennis, "Phase Singularities in Isotropic Random Waves," *Proc. R. Soc. London A* **456**, pp. 2059–2079, 2000.

9. E.J. Galvez and M.A. O'Connell, "Existence and Absence of Geometric Phases Due to Mode Transformations of High-Order Modes," *Proc. SPIE* **5736**, pp. 166–172, 2005.